Energy Materials

Supplementary Materials

Promoted de-solvation effect and dendrite-free Zn deposition enabled by *in-situ* formed interphase layer for high-performance zinc-ion batteries

Binxin Song[1,2], Qiongqiong Lu[1,3,*], Xinyu Wang[2], Peixun Xiong[4,*]

[1]Henan Key Laboratory of Advanced Conductor Materials, Institute of Materials, Henan Academy of Sciences, Zhengzhou 450001, Henan, China.

[2]Institute of Materials and Technology, Dalian Maritime University, Dalian 116026, Liaoning, China.

[3]Key Laboratory of Advanced Energy Materials Chemistry (Ministry of Education), Nankai University, Tianjin 300071, China.

[4]Inorganic Chemistry I, Technische Universität Dresden, Dresden 01069, Germany.

[*]**Correspondence to:** Dr. Qiongqiong Lu, Henan Key Laboratory of Advanced Conductor Materials, Institute of Materials, Henan Academy of Sciences, 11 Changchun Road, Zhengzhou 450001, Henan, China; Key Laboratory of Advanced Energy Materials Chemistry (Ministry of Education), Nankai University, 94 Weijin Road, Tianjin 300071, China. E-mail: qqlu@hnas.ac.cn; Dr. Peixun Xiong, Inorganic Chemistry I, Technische Universität Dresden, Bergstrasse 66, Dresden 01069, Germany. E-mail: xiongpeixun@163.com

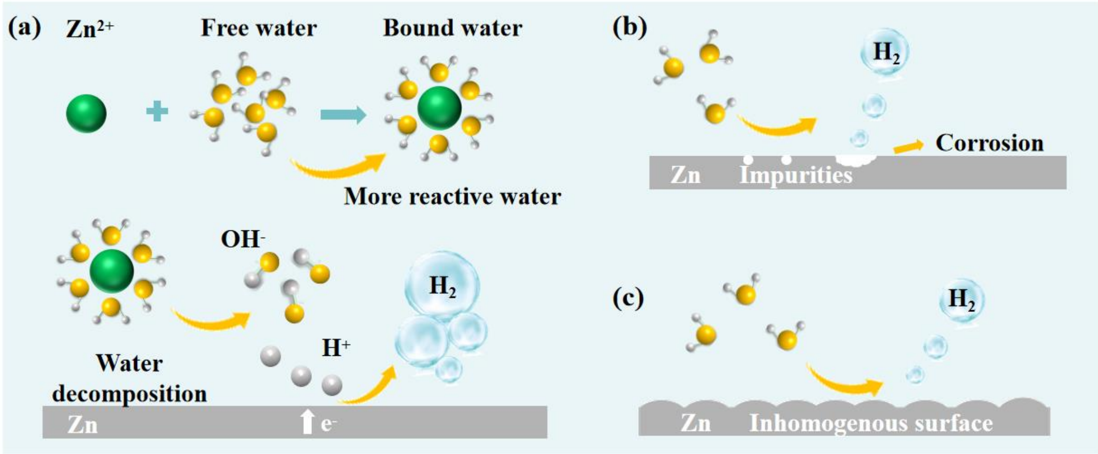

Figure S1. (a-c) The mechanism of HER for Zn metal in aqueous electrolytes

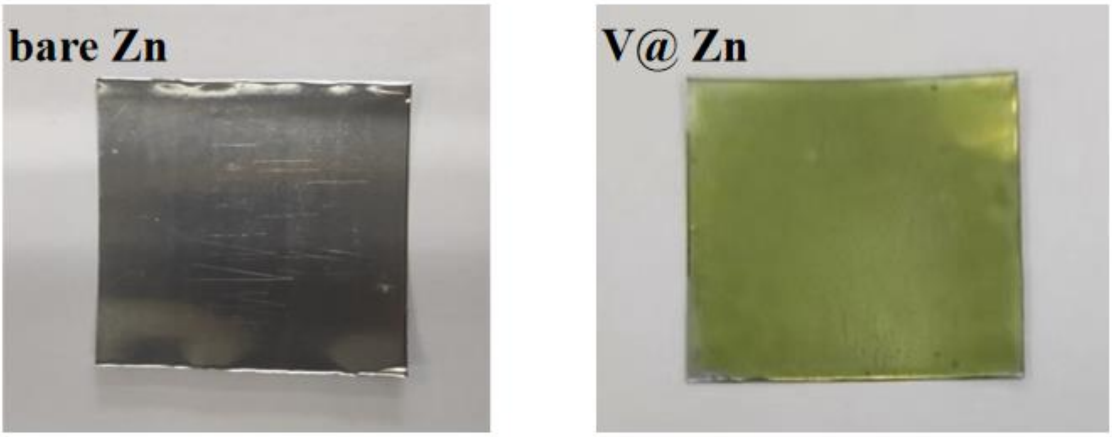

Figure S2. Optical images of pure Zn foil and V@Zn.

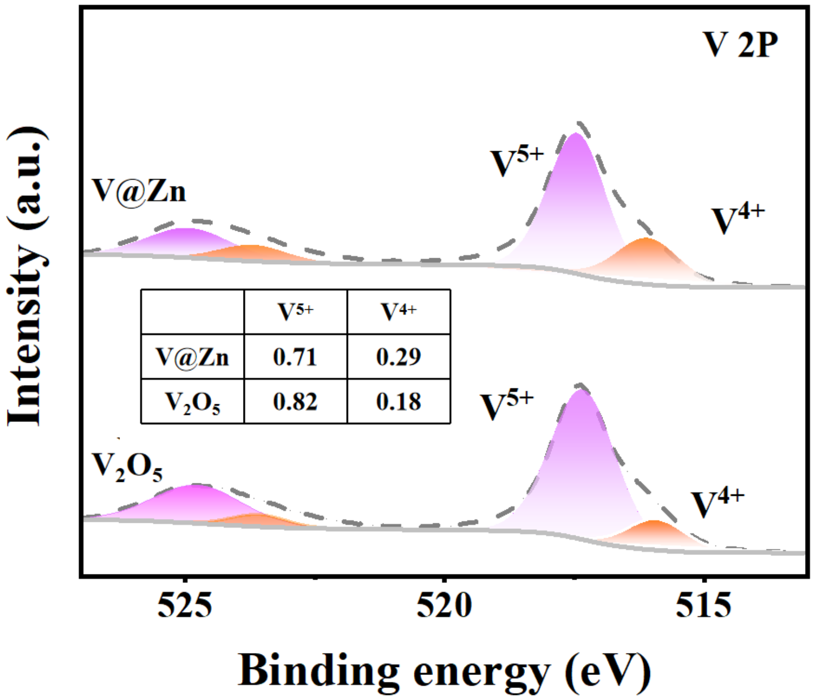

Figure S3. XPS spectrum of V_2O_5 and V@Zn.

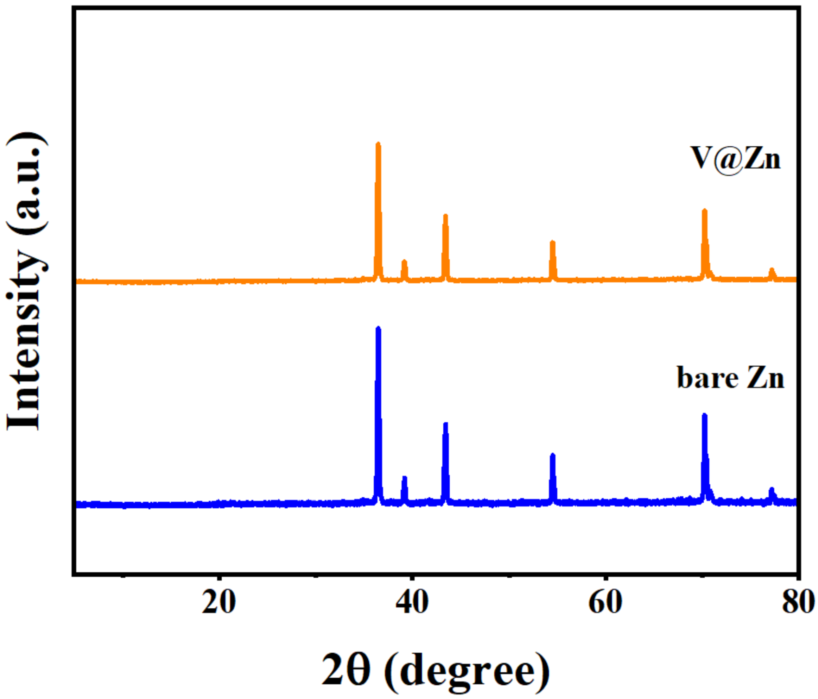

Figure S4. XRD pattern of the bare Zn electrode and V@Zn electrode.

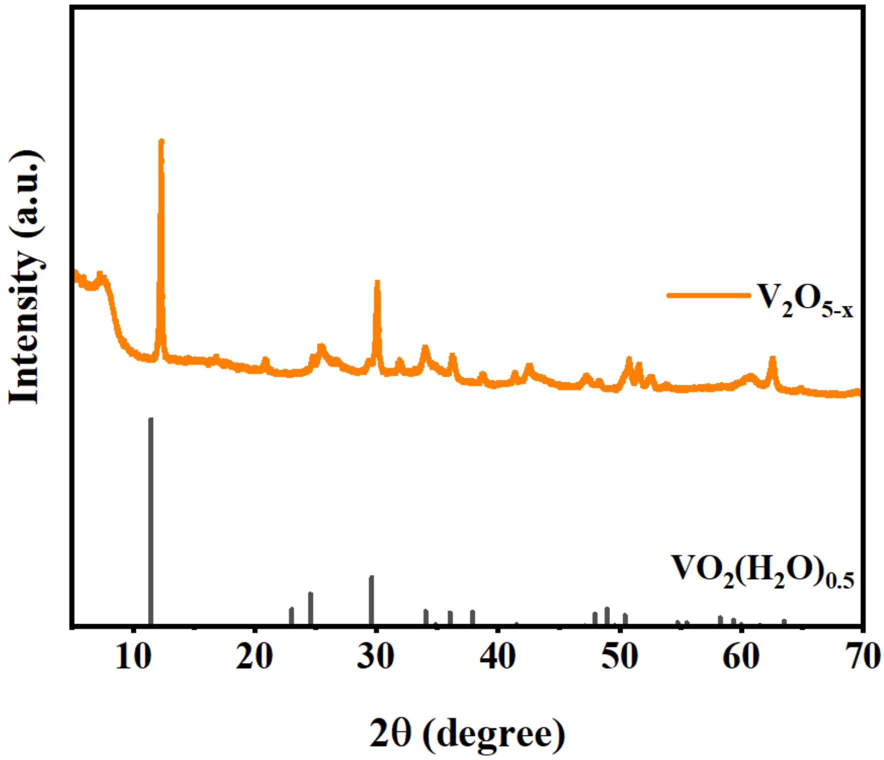

Figure S5. XRD pattern of the V_2O_{5-x}.

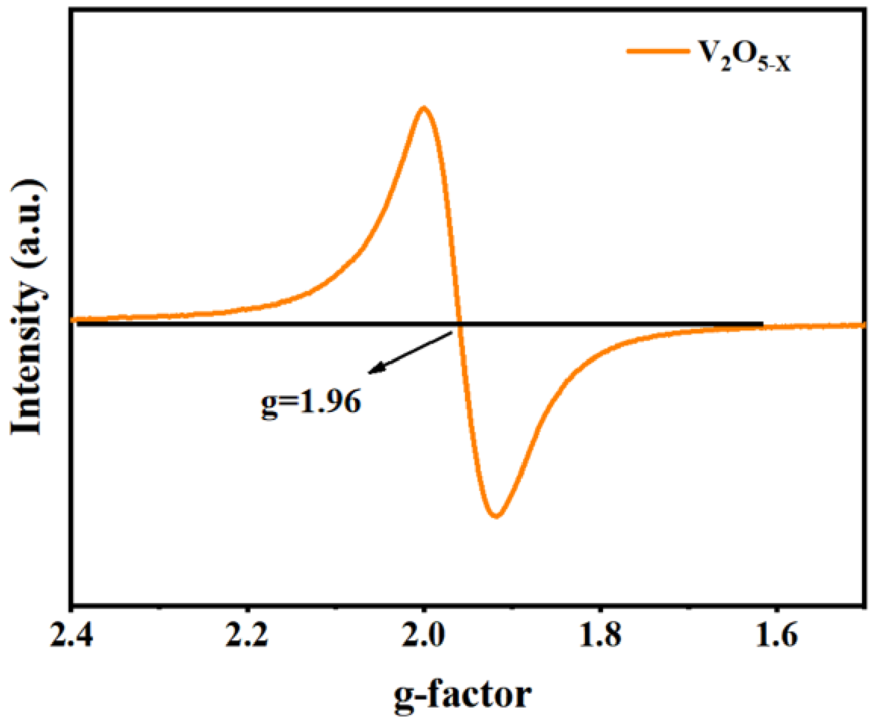

Figure S6. EPR spectrum of V_2O_{5-x} at room temperature.

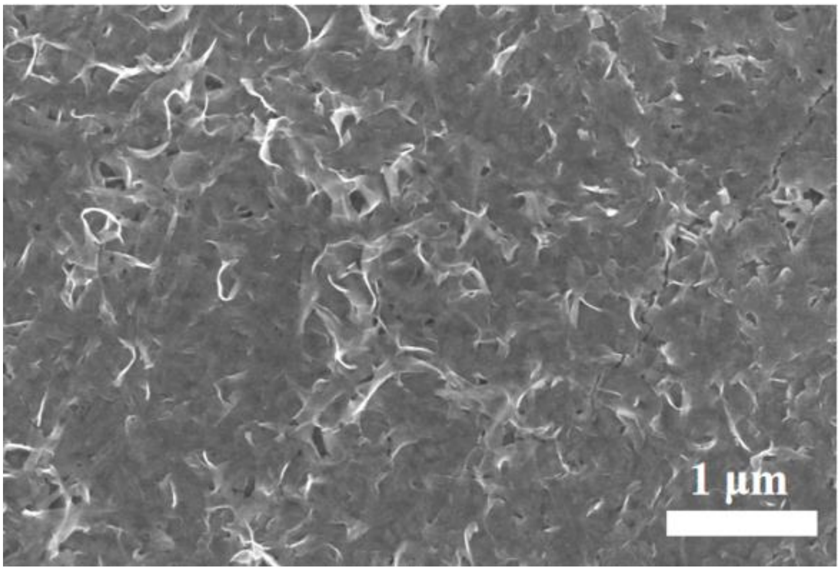

Figure S7. SEM image of V@Zn.

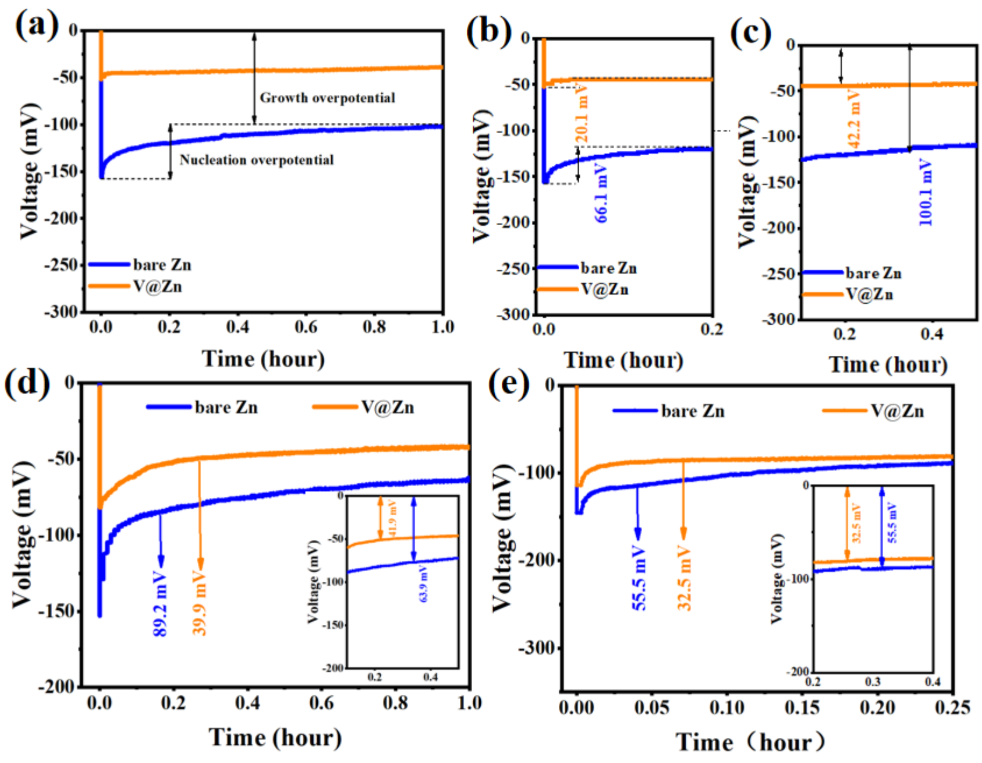

Figure S8. (a) Voltage-time curve of Zn nucleation on bare Zn and Mn@Zn electrodes at 0.5 mA cm^{-2}, Comparison of (b) nucleation overpotential and (c) deposition potential of V@Zn and Zn electrodes at a current density of 0.5 mA cm^{-2}. Comparison of nucleation overpotential and deposition potential of V@Zn and Zn electrodes at a current density of (d) 1 mA cm^{-2} and (e) 3 mA cm^{-2}.

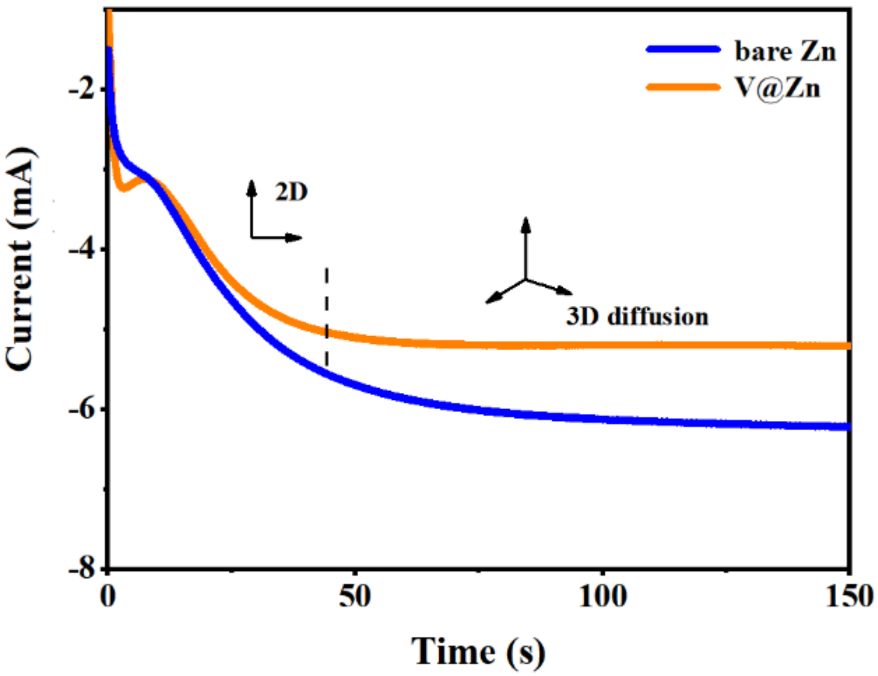

Figure S9. Chronoamperograms of bare Zn and V@Zn at -150 mV overpotential.

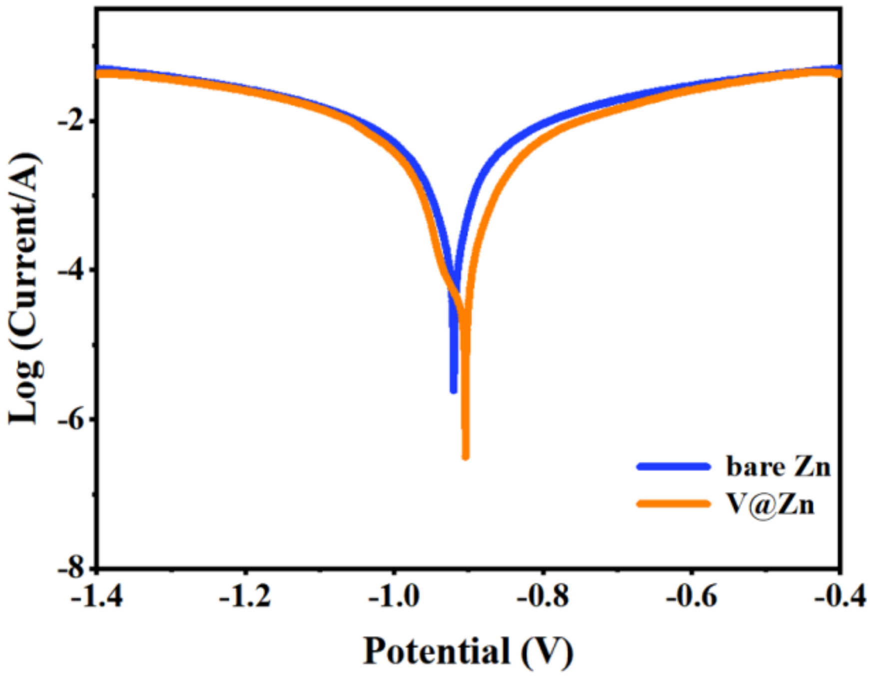

Figure S10. Linear polarization curves of the bare Zn and V@Zn electrodes.

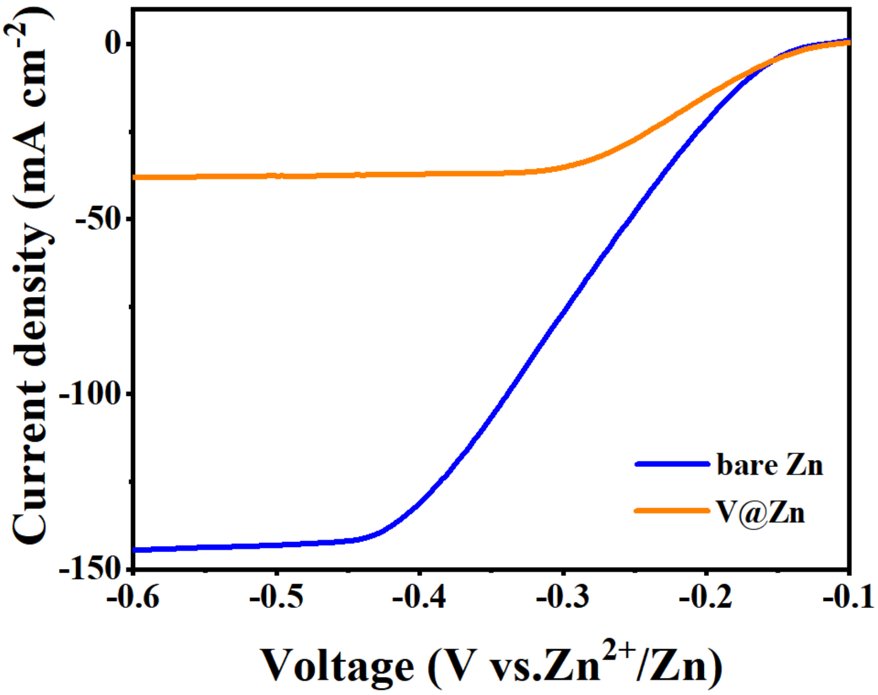

Figure S11. The hydrogen evolution (HER) performance of bare Zn and V@Zn.

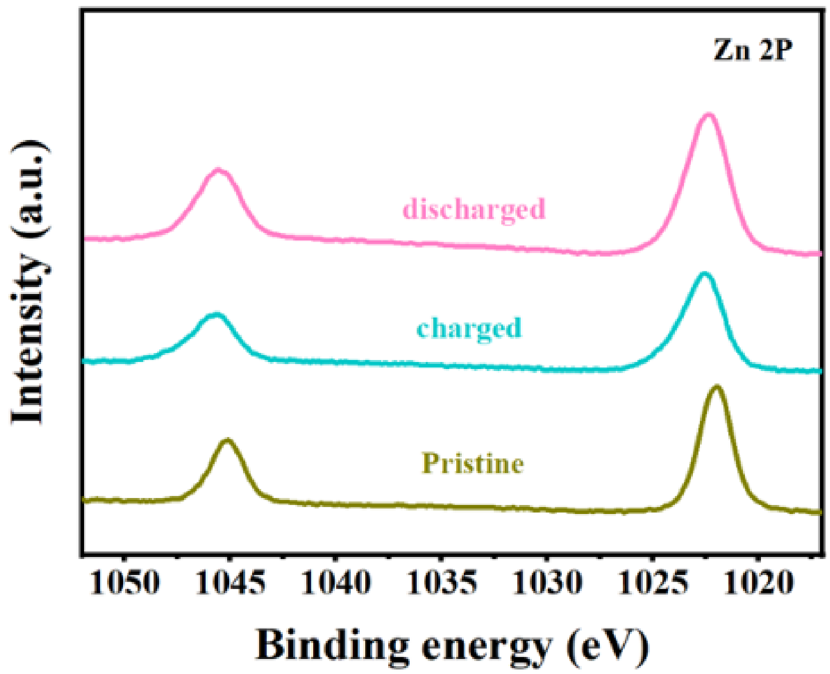

Figure S12. XPS spectra of Zn 2p of the V@Zn electrodes in pristine, discharged and charged states.

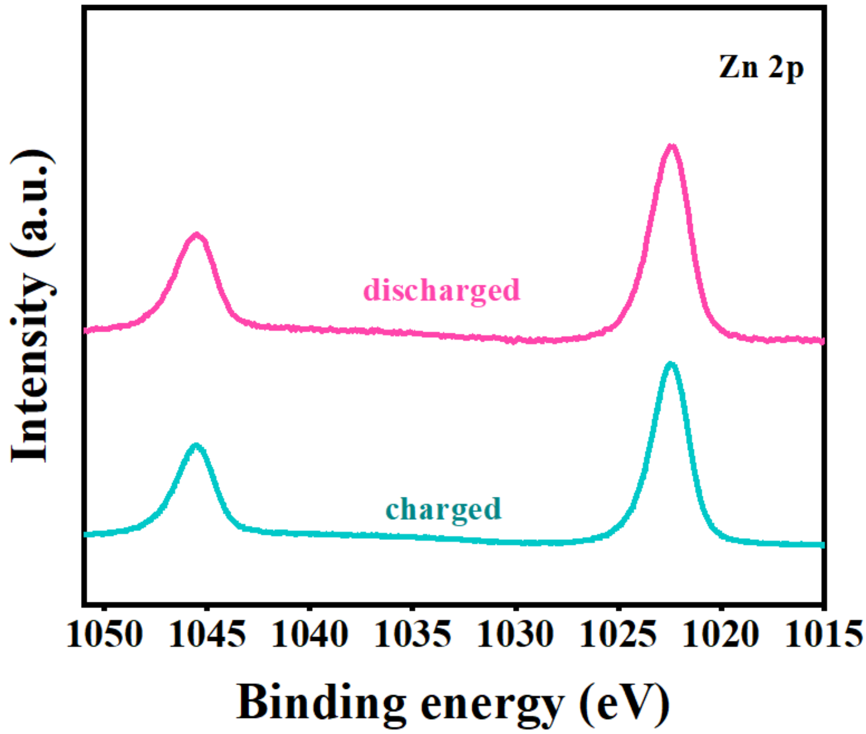

Figure S13. XPS spectra of Zn 2p of the bare Zn electrodes in discharged and charged states.

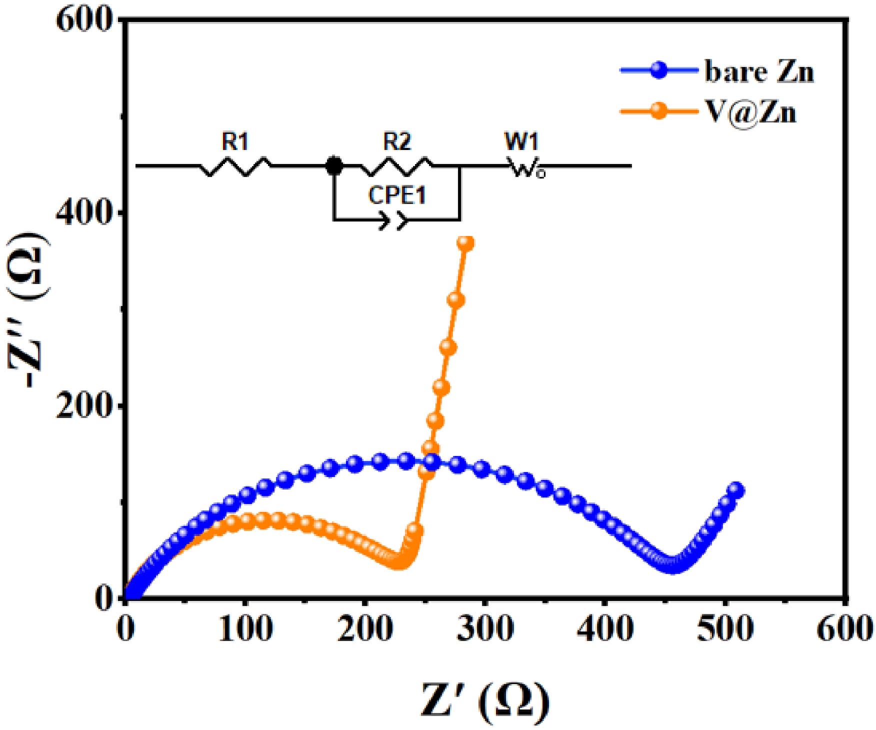

Figure S14. EIS plots of bare Zn//Zn and V@Zn//V_2O_5 full cells.

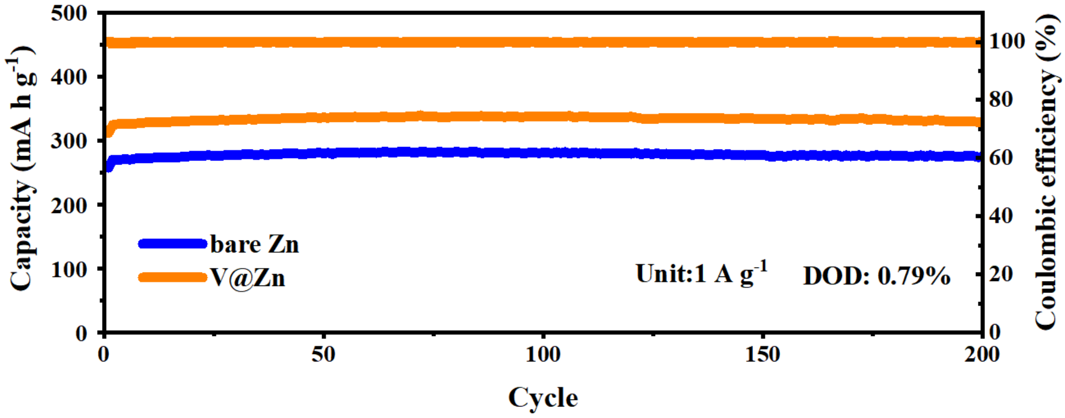

Figure S15. Long-term cycling performance at 1 A g^{-1}.

Table S1. **Performance comparison of various protection strategies for zinc-ion batteries**

Anode	Thickness	Cycling performance ($mA\ cm^{-2}$, $mAh\ cm^{-2}$)	Capacity ($mAh\ g^{-1}$)	Reference
V@Zn	230 nm	1400 h (1, 1)	276 (2500 cycles)	This work
V@Zn	230 nm	720 h (3, 1)	276 (2500 cycles)	This work
V@Zn	230 nm	320 h (5, 1)	276 (2500 cycles)	This work
Zn@LDO	10 μm	600 h (2, 1)	160 (1600 cycles)	[1]
NGO@Zn	150 μm	500 h (1, 1)	62 (3000 cycles)	[2]
PTO@Zn	2 μm	1300 h (1, 1)	198 (200 cycles)	[3]
Zn@ZVO	20 μm	1100 h (10, 1)	192 (1000 cycles)	[4]
Zn@PANI	170 nm	500 h (3, 1.5)	150 (1000 cycles)	[5]
Zn@Ag	8 μm	600 h (1, 1)	75 (800 cycles)	[6]
N-C/Zn	20 μm	800 h (2, 2)	162 (500 cycles)	[7]
hmTO-Zn	56 μm	800 h (0.25, 0.05)	102 (5000 cycles)	[8]
MOF@Zn	1 μm	700 h (0.5, 0.5)	110 (1200 cycles)	[9]
PANZ@Zn	11 μm	1100 h (1, 1)	255 (1000cycles)	[10]

References

1. Lu X, Zhao C, Chen A,, et al. Reducing Zn-ion concentration gradient by SO_4^{2-}-immobilized interface coating for dendrite-free Zn anode. *Chem Eng J* 2023;451:138772. DOI: 10.1016/j.cej.2022.138772
2. Hao Y, Zhou J, Wei G, et al. Artificial N-doped graphene protective layer enables stable Zn anode for aqueous Zn-ion batteries. *ACS Applied Energy Materials* 2021;4:6364-73. DOI: 10.1021/acsaem.1c01306
3. Liu S, Yu Q, Liu H, et al. A multifunctional protective layer filled with 2D anionic nanosheets enabling a dendrite-free zinc anode. *Inorg Chem Front* 2024;11:1135-44. DOI: 10.1039/d3qi01981k
4. Zhou Y, Li G, Feng S, et al. Regulating Zn ion desolvation and deposition chemistry toward durable and fast rechargeable Zn metal batteries. *Adv Sci* 2022;10:2205874. DOI: 10.1002/advs.202205874
5. Li B, Liu S, Geng Y, et al. Achieving stable zinc metal anode via polyaniline interface regulation of Zn ion flux and desolvation. *Adv Funct Mater* 2023;34:2214033. DOI: 10.1002/adfm.202214033
6. Liang Z, Zhou W, Wang W, et al. In situ formation of Zn@Ag resulted in uniform and dendrite-free zinc deposition for the zinc metal anode. *J Phys Conf Ser* 2024;2840. DOI: 10.1088/1742-6596/2840/1/012024
7. Wu C, Xie K, Ren K, Yang S, Wang Q. Dendrite-free Zn anodes enabled by functional nitrogen-doped carbon protective layers for aqueous zinc-ion batteries. *DTr* 2020;49:17629-34. DOI: 10.1039/d0dt03459b
8. Naresh N, Eom S, Hwan Jeong S, et al. Dendrite-free Zn anodes enabled by a hierarchical zincophilic TiO_2 layer for rechargeable aqueous zinc-ion batteries. *Appl Surf Sci* 2022;606:154932. DOI: 10.1016/j.apsusc.2022.154932
9. Lei L, Zhao B, Pei X, et al. Optimizing porous metal-organic layers for stable zinc anodes. *ACS Appl Mater* 2023;16:485-95. DOI: 10.1021/acsami.3c12369
10. Chen P, Yuan X, Xia Y, et al. An artificial polyacrylonitrile coating layer confining zinc dendrite growth for highly reversible aqueous zinc-based batteries. *Adv Sci* 2021;8:2100309. DOI: 10.1002/advs.202100309